ELSEVIER

Nuclear Instruments and Methods in Physics Research B 173 (2001) 441–446

NIM B
Beam Interactions with Materials & Atoms

www.elsevier.nl/locate/nimb

Monte Carlo simulation of concentration distribution at Ni_3Al–5 at.% Mg grain boundary ☆

Li-Ping Zheng [a,b,*], De-Zhang Zhu [a,b], Bing-Yao Jiang [c], Xiang-Huai Liu [c], Dou-Xing Li [d]

[a] *Shanghai Institute of Nuclear Research, Chinese Academy of Sciences, P.O. Box 800-204, 201800 Shanghai, People's Republic of China*
[b] *International Centre for Material Physics, Chinese Academy of Sciences, 110015 Shenyang, People's Republic of China*
[c] *Ion Beam Laboratory, Shanghai Institute of Metallurgy, Chinese Academy of Sciences, 200050 Shanghai, People's Republic of China*
[d] *Laboratory of Atomic Imaging of Solid, Institute of Metal Research, Chinese Academy of Sciences, 110015 Shenyang, People's Republic of China*

Received 7 March 2000; received in revised form 12 July 2000

Abstract

This work has applied the embedded atom method (EAM) to calculate concentration distribution of Mg, Ni and Al at a Ni_3Al–5 at.% Mg grain boundary, and the Mg-induced distortion energies at the grain boundary, the bulk and the free surface. The calculated concentration distributions show that Mg segregation is present with Al-depletion and Ni-enrichment at the grain boundary. The cause might be not only that at the same zone, the Mg-induced distortion energy in the site of Al is always negative and lower than that of Ni, but also that the Mg-induced distortion energy in the Al site at the grain boundary is the lowest among those at all zones.

1. Introduction

The intermetallic compound Ni_3Al has high strength at elevated temperature with a characteristic positive temperature dependence on strength over a certain temperature range [1]. This remarkable property, however, is not sufficient to make it useful for high-temperature applications because of its brittleness and unfabricability. It has been demonstrated that Mg ion implantation into Ni_3Al is very effective to improve its ductility [2,3] and its corrosion resistance in a solution of 1N H_2SO_4 [4].

At the Ni_3Al grain boundaries, the concentration distribution of Mg, Ni and Al was measured by Liu et al. [4], using electron probe microanalysis (EPMA) and electron dispersive spectrum (EDS). It was found that Mg segregation is present with the Al-depletion and the Ni-enrichment. Then, Jiang et al. [5] studied the effect of Mg on the Ni_3Al grain boundary, and explained the finding of the measurements [4]. However, to our knowledge, [5] and other simulations [10] have not given any concentration distributions of individual ele-

☆ Supported by the National Natural Science Foundation of China No 59831020

* Corresponding author. Fax: +86-21-5955-3021.

0168-583X/01/$ - see front matter
PII: S0168-583X(00)00406-7

ment at the grain boundaries. No comparison between the experimental and the simulated results are given either. This work calculates such concentration distributions and further explains why the Mg segregation is present with the Al-depletion and the Ni-enrichment at the grain boundary.

2. Interatomic potentials

2.1. Potentials for pure Ni, Al and Mg

The embedded atom method (EAM) energy of an n-particle homonuclear system is given by

$$E = \frac{1}{2}\sum_{i\neq j}^{n}\phi(r_{ij}) + \sum_{i}^{n}F\left(\bar{\rho}_i\right), \tag{1}$$

where E is the total energy of the system, r_{ij} the distance between atom i and j, and $\phi(r)$ is a pair wise interaction potential which is taken to be a Morse function,

$$\phi(r) = D_{\mathrm{M}}\{1 - \exp[-\alpha_{\mathrm{M}}(r - R_{\mathrm{M}})]\}^2 - D_{\mathrm{M}}, \tag{2}$$

where the three parameters, $D_{\mathrm{M}}, R_{\mathrm{M}}$ and α_{M}, are defined as the depth, distance to minimum, and the measure of the curvature near the minimum, respectively.

According to Foiles et al. [6], $F(\rho)$ is specified by requiring that the energy of the crystal behaves properly as the lattice constant is varied and satisfies the equation of [7].

$$E(a^*) = -E_{\mathrm{coh}}(1 + a^*)\mathrm{e}^{-a^*}, \tag{3}$$

where E_{coh} is the cohesive energy (per atom) and a^* is reduced lattice constant defined by

$$a^* = (a/a_0 - 1)/(E_{\mathrm{coh}}/9B\Omega)^{1/2}, \tag{4}$$

where a is the lattice constant, a_0 the equilibrium lattice constant, B the bulk modulus, and Ω is the equilibrium atomic volume.

The electron density function, $\rho(r)$, is taken as [6]

$$\rho(r) = r^6[\exp(-\beta r) + 2^9\exp(-2\beta r)], \tag{5}$$

where β is an adjustable parameter, r the distance between two atoms and $\bar{\rho}_i$ is the electron density at atom i, which is contributed by its all neighbors,

$$\bar{\rho}_i = \sum_{j\neq i}^{n}\rho(r_{ij}). \tag{6}$$

The potential parameters for fcc Ni and Al were determined by Chen et al. [10,11]. The potential parameters for Mg were optimized by minimizing the root-mean-square deviation between the calculated and reference properties of the hcp structure. These properties are the lattice constant, cohesive energy, the five elastic constants (C_{11}, C_{12}, C_{13}, C_{22} and C_{44}) [11], the vacancy formation energy (ΔE^f_{1v}) [11], the bond length (Re) and bond energy (De) of the diatomic molecule [12]. The cutoff distance r_{cut} is taken to be the third neighbor distance to ensure the stability of the fcc or hcp lattice structure. The optimized parameters are given in Table 1 of [5].

The stability of the hcp Mg lattice structure was checked by computing the cohesive energy of the bcc and fcc phases and it was found that the hcp structure is energetically favored over the bcc and fcc structure. The energy difference $E_{\mathrm{bcc}}-E_{\mathrm{hcp}}$ is 0.022180 eV and $E_{\mathrm{fcc}}-E_{\mathrm{hcp}}$ is 0.001861 eV.

2.2. The cross potentials

In the Ni–Al–Mg alloy sytem, there are 12 functions. The functions, Φ_{NiNi}, Φ_{AlAl}, Φ_{MgMg}, ρ_{Ni}, ρ_{Al}, ρ_{Mg}, F_{Ni}, F_{Al}, and F_{Mg} were determined from the fits to pure Ni, Al and Mg. The other three functions Φ_{NiAl}, Φ_{NiMg} and Φ_{AlMg} need to be determined. Each of them is taken as Morse function, with a cutoff distance to third neighbor. According to Chen et al. [10,11], two parameters are added in fitting the alloy properties. The scaling transformation is as follows:

$$\rho'_j = S_j\rho_j(r), \tag{7}$$

$$\bar{\rho}_i = \sum_{j\neq i}^{n}\rho'_j, \tag{8}$$

$$F_i^{\mathrm{T}}(\bar{\rho}) = F_i(\bar{\rho}/S_i) + g_i\bar{\rho}_i, \tag{9}$$

$$\phi_{ij}^{\mathrm{T}}(r) = \phi_{ij}(r) - 2g_jS_j\rho_j. \tag{10}$$

As only two of the three $\rho(r)$ functions can be independently scaled, following Chen et al., S_{Ni} is

taken to be one. The cross-potential Φ_{NiAl} and three transformation parameters: S_{Al}, g_{Ni} and g_{Al} were determined by Chen et al. [10,11]. The other cross-potentials and transformation parameters Φ_{NiMg}, Φ_{AlMg}, S_{Mg} and g_{Mg} were fitted in [5].

The potential parameters should be optimized by fitting to variety of experimental data on Ni–Mg alloy and Al–Mg alloy. Since the alloy structures are rather complex, the linear Muffin Tin Orbital (LMTO) [10] was used to get these properties, including lattice constant, cohesive energy and elastic constants, listed in Table 2 of [5].

Φ_{NiMg} and S_{Mg} were optimized using LMTO data on Ll_2 phase Ni_3Mg and B_2 phase NiMg. Φ_{AlMg} was optimized using LMTO data on Ll_2 phase Al_3Mg and B_2 phase AlMg. Table 3 of [5] shows the optimized parameters.

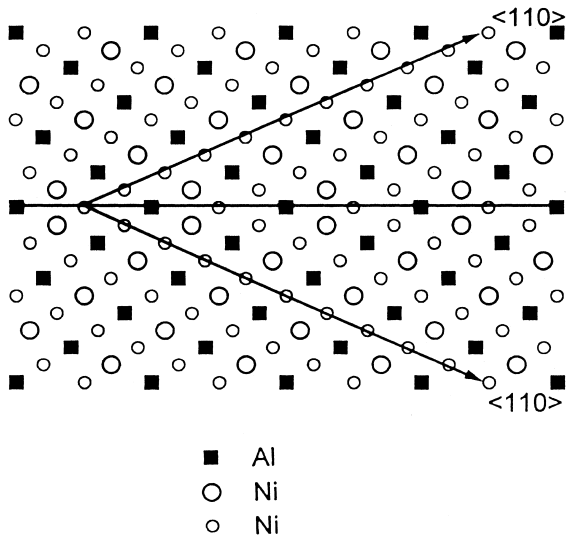

Fig. 1. $Ni_3Al[0\,0\,1]/\sum 5\langle 2\,1\,0\rangle/36.87°$ symmetric tilt boundary.

3. Monte Carlo simulation

3.1. General consideration

Monte Carlo method was used to relax the grain structure to minimum energy configuration. The unrelaxed, starting structure of the grain boundary was assumed to be the coincidence site lattice (CSL) model. There are only three stoichiometry of the grain boundaries due to the two types of planes existing in Ni_3Al for the [0 0 1] symmetric tilt boundaries. The (100%Ni\100%Ni) boundary is Ni rich and the (50%Ni\50%Ni) boundary is Al rich. The (100%Ni\50%Ni) boundary has the same stoichiometry as bulk Ni_3Al, so the (100%Ni\50%Ni) $[0\,0\,1]/\sum 5\langle 2\,1\,0\rangle/36.87°$ symmetric tilt boundary structure of Ni_3Al was selected, as shown in Fig. 1.

In many materials, the process of diffusion or atomic transport depend on the generation and migration of vacancies or interstices. The Monte Carlo simulation is based on the basic assumption described above, and two special features employed in the present model are as follows:

(a) For a given Ni_3Al–Mg system, Mg atoms are selected in order. One of its neighbors or interstices is selected randomly and is replaced by the Mg atom. The position left by Mg is filled by the original lattice atom or interstice. The atomic positions fixed at the equilibrium should correspond to E_{min} (the minimum of the system energy), i.e., E_{min} is the necessary condition for them. During relaxation, the change in the system energy, ΔE, is calculated to search E_{min}. If $\Delta E < 0$, i.e., the move would bring the system to a state of lower energy, the move is allowed. If $\Delta E > 0$, the Boltzmann factor [8] judges whether the move would be allowed for admitting statistical fluctuation influence or not allowed. Thus, the above simulation process continues until E_{min} appears, corresponding to E_{min}, the atomic positions fixed at the equilibrium would be obtained.

(b) No local atomic relaxation is allowed.

3.2. Computation cell

A schematic drawing of the computation cell is shown in Fig. 2. The calculation cell used in the present study is finite and it is composed of three regions. The dotted lines in the X–Z plane delineate the grain boundary plane. In region I, the atoms are allowed to exchange their sites and the solute concentration changes during simulation. In region II, the atoms exchange their sites, but the average solute concentration is kept constant during the entire simulation period. In region III,

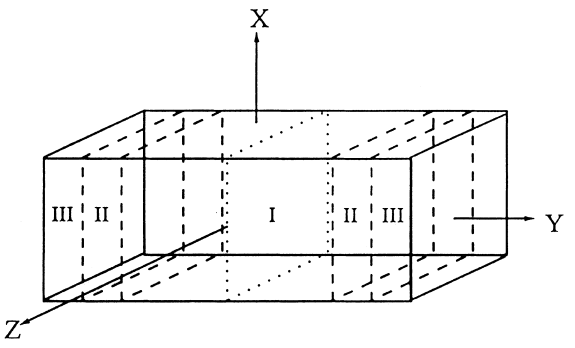

Fig. 2. Schematic drawing of the computation cell in Monte Carlo model X:⟨1 2 0⟩, Y:⟨2 1 0⟩, Z:⟨0 0 1⟩.

the atoms are fixed on their lattice site and the function of region III is to exert bulk-like forces on the atoms in region I and II. For this boundary, the computation cell includes a total of 4623 atoms in region I, 2101 atoms in region II and 14 291 atoms in region III. However, usual periodic boundary conditions were employed along X- and Z-directions [9]. The initial bulk concentration of Mg atoms in the computation cell is given as 5 at.% and dispersed randomly homogeneously.

In our system of 21 015 atoms, it takes about 1.05×10^7 MC steps to achieve the equilibrium.

4. Results and discussion

The present calculations show the concentration distributions of enriched-Mg (Fig. 3), enriched-Ni and depleted-Al (Fig. 4) at the Ni_3Al–5 at.% Mg grain boundary, and also show the Mg-induced distortion energies at the grain boundary, the bulk and the free surface (Table 1). Note (Fig. 5) that (the Mg-induced distortion energy in the site of Al(or Ni)) = (the energy of the Mg atom in the site of the Al(or Ni))−(the energy of the Al(or Ni) atom in this site). Also note that the distortion energy is correlated to both the energy caused by the atomic size and the bounding energy. Implanted Mg atoms can induce lattice distortion of Ni_3Al and mostly occupy the lattice sites of either Al or Ni. Thus, an interesting question arises whether the Mg atom prefers to substitute the Al or the Ni atoms. Calculations of the Mg-induced distortion energies can answer this question.

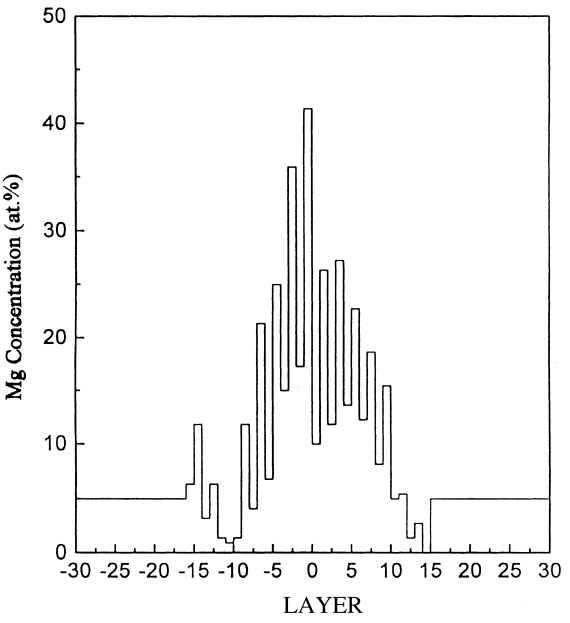

Fig. 3. Solute concentration versus position of atomic layer for the $Ni_3Al[0\,0\,1]/\sum 5\langle 2\,1\,0\rangle/36.87°$ symmetrical grain by simulations. An atomic layer means in the region between y and $y + \Delta y$, where y is the perpendicular distance from the grain boundary plane and Δy is 0.07976 nm.

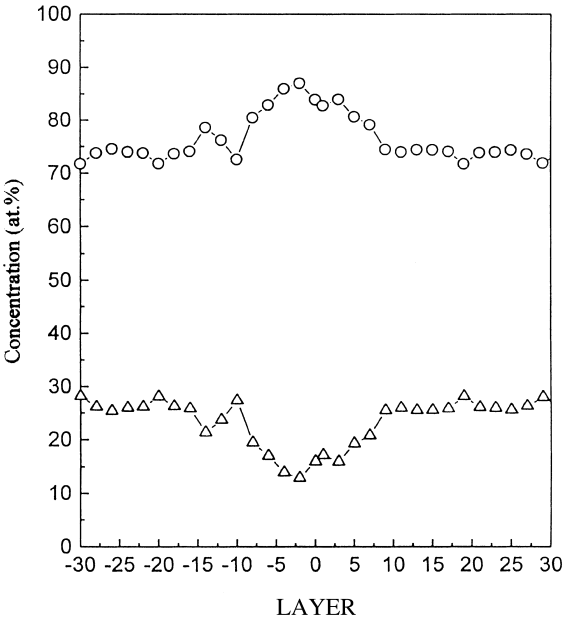

Fig. 4. Component profiles versus position of atomic layer for the Ni3Al[0 0 1]/$\sum$ 5⟨2 1 0⟩/36.87° symmetrical grain boundary by simulations. ○: Ni; Δ: Al.

Table 1
The Mg energy and Mg-induced distortion energies at the grain boundary, the bulk and the free surface for the Ni_3Al–5 at.% Mg alloy

Zone	Site	Mg energy (eV/atom)	Distortion energy (eV/atom)
Surface	Ni	−8.41	−0.42
	Al	−8.68	−0.43
Bulk	Ni	−18.71	+0.24
	Al	−20.78	−1.79
Grain boundary	Ni	−16.91	−0.63
	Al	−19.97	−2.74

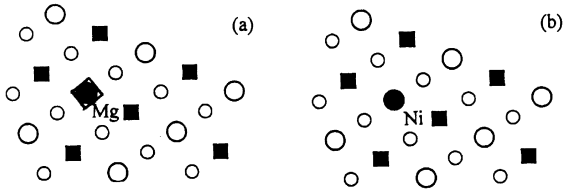

Fig. 5. Rough drawing for calculating the energy of the Mg atom (◆) in the site of Ni (a), and the energy of the Ni atom (●) in this site (b).

For the Ni_3Al–5 at.% Mg alloy, Table 1 indicates that at the same zone, the Mg-induced distortion energy in the site of Al is always negative and lower than that of Ni (here, it is emphasized that if an implanted atom attempts to occupy the site of the target atom, its induced distortion energy in this site should be, at least, negative). Therefore, the Mg atom prefers to substitute the Al atom rather than the Ni atom. This indication is consistent with the well-known regulation of the atomic radius (0.160 nm for Mg, 0.125 nm for Ni and 0.143 nm for Al). Reason is that the atomic radius difference between Al and Mg is less than 15%, which favor to form substitution solid solution, but that between Ni and Mg is more than 15%, which is unfavorable to form substitution solid solution.

Besides the above indication, Table 1 also indicates that the Mg-induced distortion energy in the site of Al at the grain boundary is the lowest among those at all zones. According to two indications, it is deduced that the Mg atom segregates preferentially to the grain boundary rather than to the bulk and the free surface, and favors to occupy the site of Al at the grain boundary. This deduction may explain why the Mg segregation is present with the Al-depletion and the Ni-enrichment at the Ni_3Al grain boundary, as shown in the measurements [4].

It is complicated to describe the diffusion process among the grain boundary, the bulk and the free surface. For simplification, the present work describes this process, only between the grain boundary and the bulk. It exhibits that during relaxation, i.e., the studied system changes from the starting structure to the equilibrium one with minimum energy configuration, the Mg atoms segregate to and accumulate around the grain boundary, where the atomic number ratio of Al to Ni decreases, correspondingly.

As mentioned above, at the Ni_3Al–5 at.% Mg grain boundary, the concentration distributions of enriched-Mg, enriched-Ni and depleted-Al, at the equilibrium, are shown in Figs. 3 and 4, respectively. Particularly, the Mg atoms are concentrated within the first ten layers from the central atomic layer (the zero layer corresponding to the grain boundary plane) and their distribution is approximately symmetrical with respect to this layer, as shown in Fig. 3. The concentration distributions in Figs. 3 and 4 are similar to those in Figs. 3 and 5 of the measurements [4], separately.

5. Summary

The embedded atom method (EAM) is used to calculate the concentration distributions at the Ni_3Al–5 at.% Mg grain boundary and the Mg-induced distortion energies at the grain boundary, the bulk and the free surface. The present calcu-

lations show not only that at the same zone, the Mg-induced distortion energy in the site of Al is always negative and lower than that of Ni, but also that the Mg-induced distortion energy in the site of Al at the grain boundary is the lowest among those at all zones. These results may explain why form the concentration distributions of enriched-Mg (Fig. 3), enriched-Ni and depleted-Al (Fig. 4), at the equilibrium.

References

[1] C.T. Liu, J.O. Stiegler, Science 226 (1984) 636.
[2] K. Aoki, O. Izumi, J. Jpn. Inst. Met. 43 (1979) 1190.
[3] J. Zhu, Z.Y. Cheng, H.Q. Ye, Scripta Metall. 23 (1989) 1537.
[4] X.H. Liu, B.Y. Jiang, X. Wang, G.Q. Yang, S.C. Zou, J. Sun, A. Schraer, W. Ensinger, G.K. Wolf, S. Kalbitzer, K. Takahashi, M. Iwaki, S. Taniguchi, Nucl. Instr. and Meth. B 80/81 (1993) 221.
[5] B.Y. Jiang, X.H. Liu, S.C. Zou, J. Sun, J. Wang, J. Mater. Res. 13 (1998) 1741.
[6] S.M. Foiles, M.I. Baskes, M.S. Daw, Phys. Rev. B 33 (1986) 7983.
[7] J.H. Rose, J.R. Smith, F. Guinea, J. Ferrante, Phys. Rev. B 29 (1984) 2963.
[8] N. Metropolis, A.W. Rosenbluth, M.N. Rosenbluth, A.H. Teller, E. Teller, J. Chem. Phys. 21 (1953) 1087.
[9] H.K. Chang, R.S. Weidmam, J.K. Lee, Surf. Sci. 144 (1984) 230.
[10] S.P. Chen, A.F. Voter, R.C. Albers, A.M. Boring, P.J. Hany, J. Mater. Res. 5 (1990) 955.
[11] S.P. Chen, D.J. Srolovitz, A.F. Voter, J. Mater. Res. 4 (1989) 76.
[12] M.S. Daw, M.I. Baskes, Phys. Rev. B 29 (1984) 6443.